Energy Conversion and Management 134 (2017) 221–234

Contents lists available at ScienceDirect

Energy Conversion and Management

journal homepage: www.elsevier.com/locate/enconman

Development and assessment of a novel integrated nuclear plant for electricity and hydrogen production

Maan Al-Zareer *, Ibrahim Dincer, Marc A. Rosen

Clean Energy Research Laboratory, Department of Automotive, Mechanical and Manufacturing Engineering, Faculty of Engineering and Applied Science, University of Ontario Institute of Technology, 2000 Simcoe Street North, Oshawa, Ontario L1H 7K4, Canada

ARTICLE INFO

Article history:
Received 2 November 2016
Received in revised form 1 December 2016
Accepted 3 December 2016
Available online 24 December 2016

Keywords:
Hydrogen production
Copper-chlorine cycle
Thermochemical cycle
Energy
Exergy
Nuclear power plant

ABSTRACT

A novel nuclear-based integrated system for electrical power and compressed hydrogen production is proposed. The hydrogen is produced through the four-step Cu-Cl cycle for water decomposition. A Rankine cycle is used to generate the power, part of which is used for the electrolysis step in the hybrid thermochemical water decomposition cycle and the hydrogen compression system. In the proposed design of the four-step thermochemical and electrical water decomposition cycle, only the hydrolysis and the oxygen production reactors receive thermal energy from the nuclear reactor. The nuclear thermal energy is delivered to the integrated system in the form of a supercritical fluid. The nuclear reactor, which is based on the supercritical water-cooled reactor, is responsible for delivering the thermal energy to the system, which is simulated using Aspen Plus and assessed with energy and exergy analyses. It is determined that the energy and the exergy efficiencies of the proposed system are 31.6% and 56.2% respectively, and that the integrated system is able to produce 2.02 kg/s of highly compressed hydrogen and 553 MW of electrical power.

1. Introduction

To maintain a comfort and living standards, various services are required such as electricity, hot water, cold water, air conditioning, and many chemicals. Conventional methods for producing these necessities use fossil fuels, which are the main contributors to carbon-based emissions, which in turn are a major contributor to global warming. The increasing demand for the above-mentioned services results has resulted in an increase in the use of fossil fuels, affecting the environment greatly [1]. According to the International Energy Agency, energy demands of the world will increase by 50% in the coming 14 years (2016–2030) and, since energy production nowadays is directly related to fossil fuel use, increased carbon-based emissions will be released to the environment [2].

The present situation is motivating the world to find and develop cleaner energy sources and hence more efficient processes. Eventually, it is expected that current fossil fuels will be replaced with sustainable energy sources. One method of reducing carbon emissions is through hydrogen production from renewable or non-carbon based resources such as solar, hydro, wave and nuclear energies. Hydrogen is a clean energy carrier that, when produced from renewable energy sources and/or non-carbon based fuels such as nuclear energy, can be used with little or no carbon emissions [3]. Hydrogen can be converted to electricity, heat, chemical fuels and other useful chemicals and the only byproduct is H_2O (water) [4]. Production of hydrogen from nuclear energy leads to few or no carbon emissions [1]. Another advantage of hydrogen production from nuclear energy now and in the future is that hydrogen will develop its own market where it can be converted to electricity through fuel cells and then sold as electricity during peak periods, or sold as a chemical fuel for transportation or chemical plants. Another advantage of nuclear-produced hydrogen is that it can help match the electrical production curve with the demand curve through either producing hydrogen as an energy storage medium during off-peak periods and or through the generation of electricity from hydrogen through fuels cells. Nuclear hydrogen production can increase the cost competitiveness of nuclear plants and make them more secure by integrating them with thermochemical cycles or hybrid thermochemical and electrical cycles or high-temperature electrical water decomposition cycles [1].

Hydrogen can be produced from nuclear energy either through electrolysis or thermochemical water decomposition or hybrid thermochemical water decomposition. Hybrid thermochemical and electrical water decomposition cycles are attracting increased attention due to their lower temperature requirements compared

* Corresponding author.
E-mail addresses: maan.al-zareer@uoit.ca (M. Al-Zareer), ibrahim.dincer@uoit.ca (I. Dincer), marc.rosen@uoit.ca (M.A. Rosen).

http://dx.doi.org/10.1016/j.enconman.2016.12.004
0196-8904/

Nomenclature

c_p	specific heat capacity at constant pressure (kJ/kg K)
ex	specific exergy (kJ/kg)
$\dot{E}x$	exergy rate (kW)
h	specific enthalpy (kJ/kg)
$\dot{m}$	mass flow rate (kg/s)
P	pressure (kPa)
$\dot{Q}$	heat rate (kW)
R	universal gas constant (kJ/mol K)
s	specific entropy (kJ/kg K)
T	temperature (°C)
$\dot{W}$	work rate (kW)

Greek letters

η	energy efficiency
ψ	exergy efficiency

Subscripts

Cu-Cl	copper-chlorine cycle
C	compressor
d	destruction
e	electrical
f	formation
gen	generation
H_2	hydrogen
HCS	hydrogen compression system
is	isentropic
in	input (flowing into system boundary)
max	maximum
net	net result
ov	overall
out	output (flowing out of system boundary)
o	reference environment conditions
$\dot{Q}$	heat flow rate
PSR	power supporting rankine cycle
ST	steam turbine
bs	boundary where heat transfer occurs
W	work
@P&T	at pressure P and temperature T

Superscripts

·	rate
LP	Low pressure
HP	High pressure

Acronyms

SCWR	Supercritical water cooled reactor
HCS	hydrogen compression system
PSR	power supporting Rankine cycle

to thermal water decomposition. Various types of hybrid thermochemical and electrical water decomposition cycles exist, and these are often differentiated based on the chemical compounds they employ and the number of steps in the cycle [1].

Investigations of hybrid thermochemical and electrical water decomposition cycles for hydrogen production have been reported, as have efforts to integrate them with other systems. One type of hybrid thermochemical and electrical water decomposition cycle uses magnesium and chlorine (the Mg-Cl cycle) [5,6]. Ozcan and Dincer [5,6] modeled and analyzed the performance of this cycle and investigated its thermal energy and electrical energy requirements. Ozcan and Dincer [6] found that the Mg-Cl cycle has energy and exergy efficiencies that allow it to compete with the other hybrid thermochemical and electrical water decomposition cycles. The Mg-Cl cycle has been integrated with a nuclear reactor, a Rankine cycle and a liquid hydrogen storage [7]. Energy and exergy analyses were performed of this integrated system and the energy and exergy efficiencies were found to be 18.6% and 31.4%, respectively [7]. An exergoeconomic analysis of the Mg-Cl cycle was also reported [8].

Another promising hybrid thermochemical and electrical water decomposition cycle is based on copper and chlorine compounds (the Cu-Cl cycle), particularly due to its relatively low-temperature requirements which permit it to be integrated with various thermal energy supply systems. Various Cu-Cl cycles exist, based on the number and type of steps comprising it [1]. Orhan et al. [9,10] examined the performance of several Cu-Cl cycles with energy and exergy analyses. The Cu-Cl cycle has also been evaluated using exergoeconomic analysis [11]. Furthermore, investigations have been reported on the integration of the Cu-Cl cycle with other hydrogen production processes [12–14]. The integration of the Cu-Cl cycle with nuclear plants that provide thermal energy has been examined [13,14], and the system energy and exergy efficiencies were found to be 45% and 10%, respectively [14]. In [14] a Cu-Cl cycle containing five main steps is considered, while a four-step Cu-Cl cycle is examined in [15].

The various Cu-Cl cycles have been investigated extensively over the last decade, using energy, exergy, exergoeconomic, exergoenviromental, analyses, and other costing methods. For example, [9,10,12,13] studied the Cu-Cl cycle itself in terms of energy and exergy analyses and evaluated its efficiency. Some examples of work done on economic aspects of the Cu-Cl cycle include the studies of [11,16]. Ref. [11] used the specific exergy costing (SPECO) method, while [16] used another costing method, exergoeconomic analysis, integrated with an enviromental viewpoint, in the form of exergoenviromental analysis. Other investigations have focused on optimizing the Cu-Cl cycle operating conditions [17,18]. In [17], a new heat exchanger network is proposed to increase the heat recovery and decrease the overall energy requirement of the cycle, while in [18], a multi-objective optimization is carried out on the cycle including energy and exergy efficiencies. However few have proposed realistic conceptual designs of the overall cycle and how the thermal energy is delivered to its reactors [19]. Some research has focused on specific parts of the overall cycle, such as reducing the auxiliary power requirements by integrating the pathways between the hydrolysis reactor and the electrolysis reactor. Also, Ref. [20] assessed the oxygen production process with energy and exergy analyses. Other reseachs proposed integrating the material flows betweenthe hydrolysis reactor and the electrolysis reactor, since both flows share the main chemical components [21]. Ref. [22] proposed and analyzed a new method for recovering the thermal energy from molten CuCl salt through casting. Experiments were carried out on different parts of the cycle, such as scaling up a reactor [23]. Other experiments have been performed on different parts of the cycle [24,25]. A number of integrated systems have been proposed, with such thermal energy sources as nuclear [14,26], solar [27–29], fossil fuels [30,31], renewable energy (only) [28], renewable energy with nuclear energy [32], and systems that integrate more than one technology [33]. Finally several review papers [34–36] have been published to inform of the most recent advances regarding the Cu-Cl cycle. Nevertheless, more work is required on integrating these cycles into systems to determine how well they perform after integration.

The aim of this paper is to propose and assess a novel nuclear-based hydrogen and electricity production plant that utilizes the four-step Cu-Cl cycle, where the hydrogen produced is in a compressed state. This work supports the Cu-Cl cycle being developed at University of Ontario Institute of Technology (UOIT). The hydrogen is compressed in the integrated system to allow it to be economically and physically stored. Since the Cu-Cl cycle is a hybrid thermochemical and electrical water decomposition cycle, the process of delivering the thermal energy to the cycle reactors is of importance, particularly since they must be maintained at 530 °C for the reactions to occur. Here, a realistic steam/water circuit is proposed to deliver heat to the four-step Cu-Cl cycle reactors. The steam/water circuit is designed to reduce losses as much as possible in a practical sense. The integrated system includes a Rankine cycle that produces the required electricity for the Cu-Cl cycle and the hydrogen compression system. Excess electrical power is delivered to the electrical grid.

2. System description

Fig. 1 shows the integrated system including the Cu-Cl cycle. Fig. 2 shows the main steps of the Cu-Cl cycle used in the integrated system. Fig. 3 shows the Aspen Plus model designed and developed for the integrated system. The integrated system consists of a supercritical water-cooled nuclear reactor (SCWR) which produces thermal energy in the form of superheated supercritical steam, a four-step Cu-Cl cycle, a supporting Rankine cycle for electricity generation, and a four-stage hydrogen compression system. A detailed description of the Cu-Cl cycle is now provided, followed by a description of the overall system and how the different systems interact. This is accompanied by a description of the Aspen Plus model for the integrated system.

The Cu-Cl cycle has been identified by the Atomic Energy of Canada Limited as a promising technology for water decomposition through a hybrid thermochemical and electrical process, with

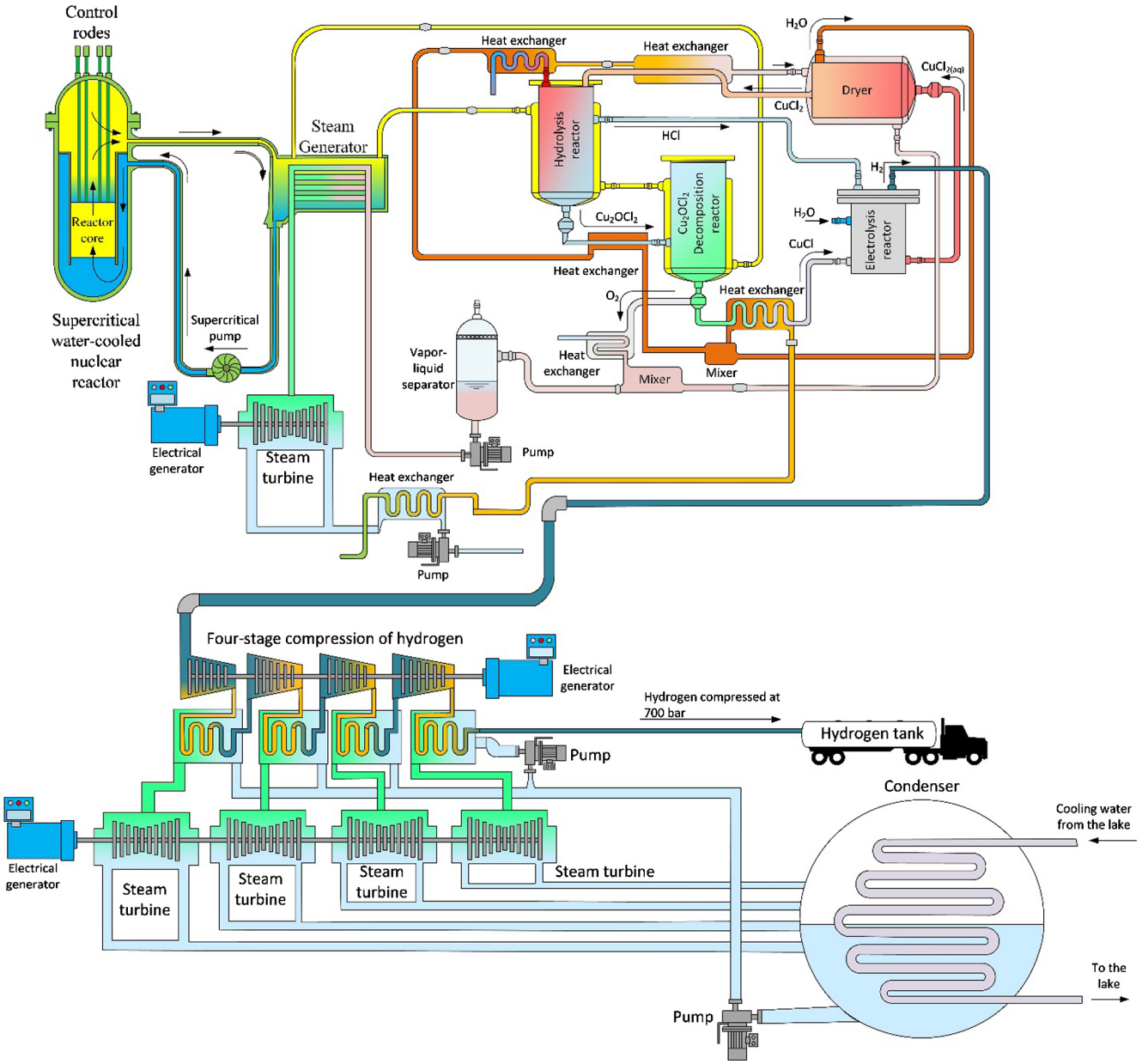

Fig. 1. Nuclear-based integrated system for electrical power and hydrogen production. The produced hydrogen is compressed in a four-stage hydrogen compression system, and the electrical power requirements of the integrated system are fulfilled by the supporting Rankine cycle.

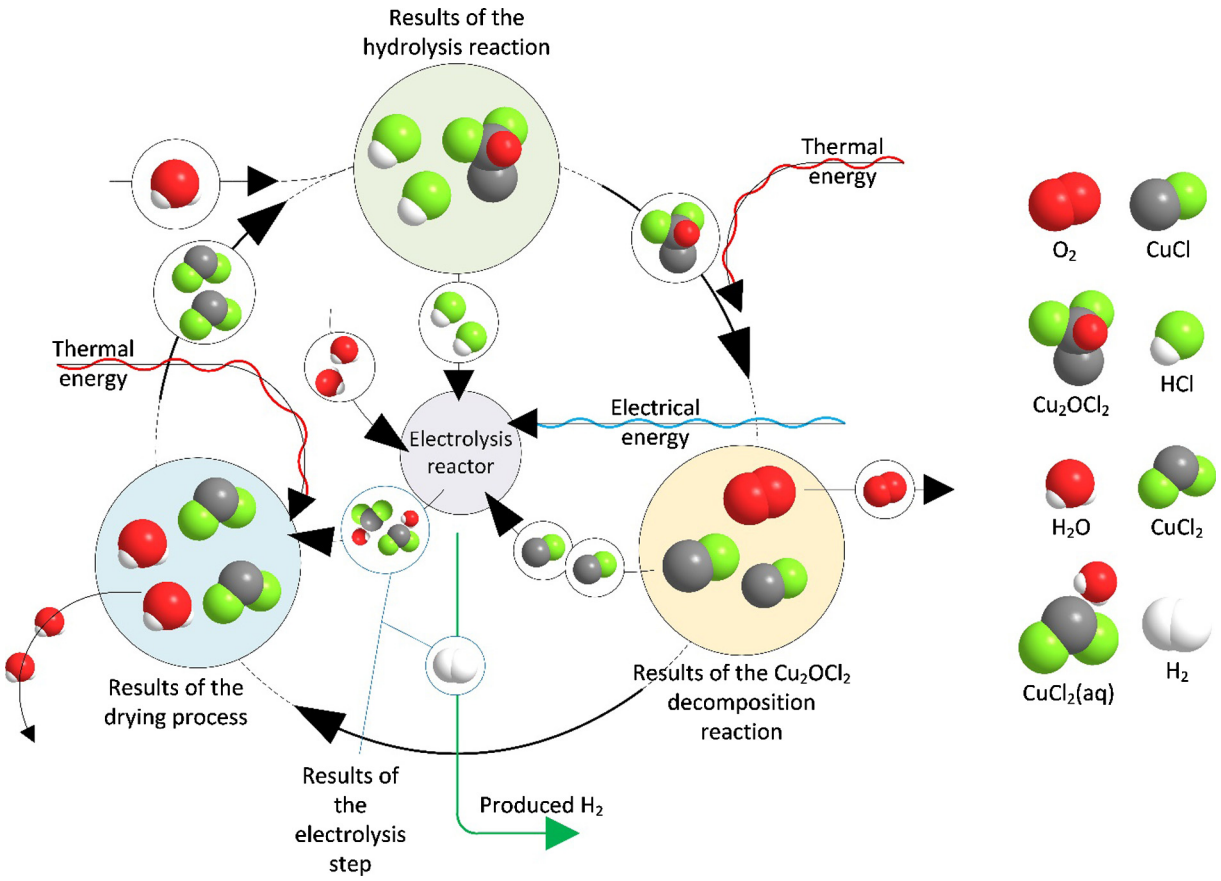

Fig. 2. Main interactions that occur in the steps of the four-step Cu-Cl cycle for thermochemical water decomposition in the integrated system.

thermal energy supplied by supercritical water-cooled nuclear reactors [18,35]. The Cu-Cl cycle has relatively low-temperature requirements, compared to high-temperature cycles, such as S-I cycle, and potentially lower material costs than competitive cycles [18,35]. UOIT, Canadian Nuclear Laboratories (formerly Atomic Energy of Canada Limited), Argonne National Laboratory in the United States, Pennsylvania State University, and other cooperating institutions are working on scaling up the Cu-Cl cycle, ultimately for industrial applications [35].

Although there are many types of Cu-Cl cycles, all share the same overall chemical reaction, which is water decomposition to hydrogen (H_2) and oxygen (O_2). The four-step Cu-Cl cycle considered here is currently investigated experimentally and theoretically at the Clean Energy Research Laboratory (CERL) in the University of Ontario Institute of Technology. The main interactions that occur in the four-step Cu-Cl cycle are illustrated in Fig. 2, and involve the following four main chemical reactions (cycle steps):

Step 1: Hydrolysis. It is required to maintain the hydrolysis reactor at a temperature between 370 °C and 400 °C: The chemical reaction follows:

$$2CuCl_2(s) + H_2O(g) \rightarrow Cu_2OCl_2(s) + 2HCl(g) \quad (1)$$

Step 2: Copper oxychloride (Cu_2OCl_2) decomposition. The decomposition reactor should be kept at temperature between 500 °C and 530 °C. The reaction is:

$$Cu_2OCl_2(s) \rightarrow 2CuCl(l) + 0.5O_2(g) \quad (2)$$

Step 3: Electrolysis. This reaction, for which the temperature needs to be less than 100 °C and higher than 25 °C, is written as follows:

$$2CuCl(aq) + HCl(g) \rightarrow H_2(g) + CuCl_2(aq) \quad (3)$$

Step 4: Drying. The aqueous cupric chloride is dried at temperatures between 80 °C and 100 °C, according to:

$$CuCl_2(aq) \rightarrow CuCl_2(s) + H_2O(g) \quad (4)$$

The energy source for the integrated system is the SCWR. In this paper, we adopt the main operating parameters for the SCWR from the literature [37]. Table 1 lists the main operating parameters for the SCWR and the integrated system. As shown in Figs. 1 and 3, the supercritical water is used without reducing its pressure (except for minor pressure losses that are neglected in the analysis, as per assumptions stated in Section 3,) and it is also used to generate steam at 100 bar pressure for the power supporting Rankine cycle (PSR cycle). Note that in the descriptions of the Aspen Plus terms for the integrated system, stream names and block names are in italics and in parentheses. First, the supercritical gas-like water exiting the SCWR (*S43*) enters the water jacket of the Cu_2OCl_2 decomposition reactor (*B6*) to provide the necessary thermal energy to the reactor, and then exits the water jacket (*S44*) and enters the hydrolysis reactor (*B1*). The supercritical fluid (*S43*) entering the water jacket of the Cu_2OCl_2 decomposition reactor (*B6*) provides the required thermal energy for the decomposition of the Cu_2OCl_2 according to Eq. (2). The supercritical fluid exits the hydrolysis reactor (*B6*) water jacket (*S46*) and then is input to the steam generator where it generates steam for the PSR cycle; the supercritical fluid in the liquid-like form (*S48*) then returns to the SCWR. As mentioned earlier, the only interaction between the supercritical fluid of the SCWR with the Cu-Cl cycle is in providing the required thermal energy for the hydrolysis and the Cu_2OCl_2 decomposition reactors; the rest of the thermal energy

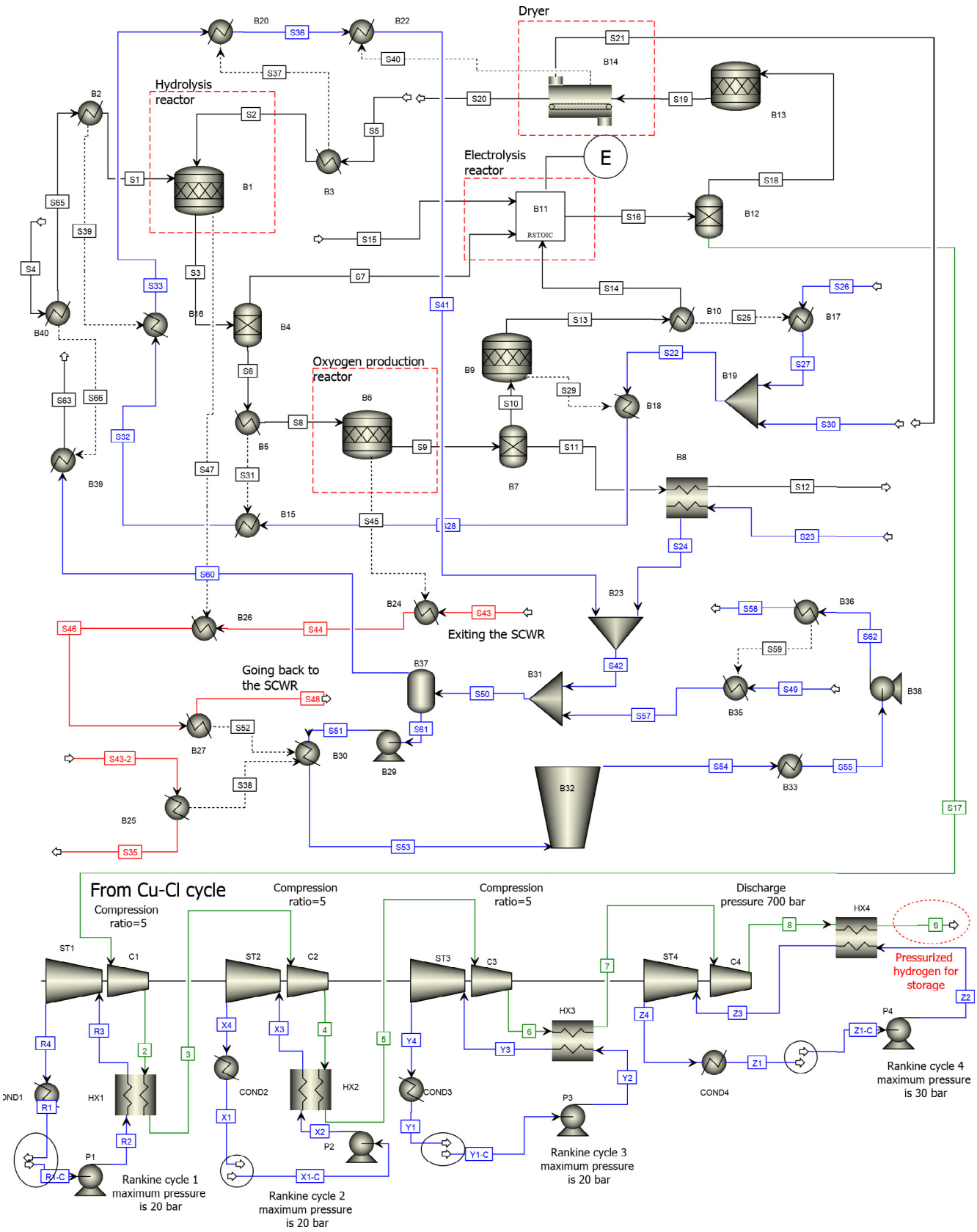

Fig. 3. Aspen Plus flow sheet for simulation of the integrated nuclear-based electrical power and hydrogen production plant.

necessary for the remaining reactors or heat exchangers is provided through heat recovery from other heat producing devices in the cycle. The heating water path inside the reactors water jackets and in the Cu-Cl cycle heat exchangers is through the steam circuit. The steam circuit first phase (absorbing thermal energy) starts with water entering at ambient conditions (*S26*) and being

Table 1
Main parameters in the proposed integrated system, consisting of SCWR, Cu-Cl cycle, supporting combined cycle, and hydrogen compression system (Aspen Plus blocks or stream names are listed in parentheses and refer to the Aspen Plus model in Fig. 3).

Subsystem	Parameter	Value	Unit	Source
SCWR	Temperature of steam exiting reactor (S43)	625	°C	[37,39]
	Temperature of water returning to reactor (S48)	350	°C	[37,39]
	Operating pressure of nuclear reactor	25	MPa	[37,39]
	Thermal energy output	2540	MW	[37,39]
	Supercritical steam mass flow rate	1320	kg/s	[37,39]
	T_{max} cladding	850	°C	[37,39]
Cu-Cl cycle	Four-step hybrid thermochemical and electrical water decomposition cycle			
	Hydrolysis reactor (B1) operating temperature	400	°C	[15,17]
	Hydrolysis reactor (B1) operating pressure	1	bar	[15,17]
	Oxygen production reactor (Cu_2OCl_2 decomposition reactor) (B6) operating temperature	530	°C	[15,17]
	Oxygen production reactor (Cu_2OCl_2 decomposition reactor) (B6) operating pressure	1	bar	[15,17]
	Electrolysis reactor (B11) operating temperature	25	°C	[15,17]
	Electrolysis reactor (B11) operating pressure	1	bar	[15,17]
	Electrolysis reactor (B11) electrical unit energy requirements	55.0	kJ/mol H_2	[13,15]
	Amount of H_2O added to the electrolysis reactor.	20	mol	
	Dryer (B14) operating temperature (higher than required to superheat the evaporated water)	110	°C	
	Dryer (B14) drying temperature	100	°C	[15,17]
	Dryer (B14) operating pressure	1	bar	[15,17]
	Solid phase properties of the materials in the Cu-Cl cycle are reported in Table 2			
Hydrogen compression system	Hydrogen final pressure	700	bar	[40,41]
	Number of compression stages	4		
	Pressure ratio of each stage except final stage	5		
	Rankine cycle connected to intercoolers			
	RC1 operating pressure	20	bar	
	RC2 operating pressure	20	bar	
	RC3 operating pressure	20	bar	
	RC4 operating pressure	30	bar	
	$\eta_{is,C}$	0.72		[42]
	$\eta_{is,ST}$	0.72		[42]
Supporting Rankine cycle	Rankine cycle operating pressure	100	bar	
	$\eta_{is,ST}$	0.72		[42]

heated by the cooling solidified CuCl (*S13*) to (*S14*) through the heat exchanger (*B17* and *B10*) to produce a saturated mixture (*S27*). Then S27 is mixed (in mixer *B19*) with the steam (*S21*) exiting the dryer (*B14*), resulting in saturated steam (*S22*) that absorbs the latent heat released during the solidification of the molten CuCl (*S10*) and produces superheated steam (S28). The second phase begins when the superheated steam (*S28*) heats the Cu_2OCl_2 (*S6*) to the operating temperature of the Cu_2OCl_2 decomposition reactor (*B6*) before entering the Cu_2OCl_2 decomposition reactor. Then it heats the water before entering the hydrolysis reactor and also heats the solid $CuCl_2$ (in heat exchanger *B20* and *B3*) to the operating temperature of the hydrolysis reactor. The heating water exiting B20 provides the necessary thermal energy to the dryer (*B14*) and then mixes with heated water (*S24*) exiting the water and oxygen heat exchanger (*B8*) and the mixture (*S42*) is conveyed to the PSR cycle.

The PSR cycle receives the saturated mixture water with small vapor fraction and mixes it with water that recovered heat from water exiting the turbine to produce lower quality water (*S50*). This water enters a vapor-liquid separator, recovering part of the thermal energy in the vapor exiting the vapor-liquid separator by preheating water from ambient conditions (*S4*). The liquid exiting the vapor-liquid separator (*S61*) is pumped to 200 bar and then superheated by the supercritical fluid to produce superheated steam at 621 °C (*S53*). This superheated steam expands through the steam turbine (*B32*) to produce electrical power that is used to cover the electrolysis reactor needs plus the needs for the hydrogen compression system (HCS) and other work consuming devices such as pumps.

The four-stage HCS compresses the hydrogen produced from the Cu-Cl cycle to a pressure of 700 bar. The first three stages have a compression ratio of 5 and the fourth stage has a discharge pressure of 700 bar. The produced hydrogen (S17) enters the HCS first compression stage, which compresses the hydrogen from 1 bar to 5 bar; the temperature of the hydrogen rises from 25 °C to 291 °C across the first compression stage. The hydrogen exiting each compression stage is cooled in heat exchangers, which act as a steam generator for the bottoming Rankine cycles that are added, to recover the heat and reduce the overall electrical power required to compress the hydrogen. The remaining three compression stages use the same procedure to finally produce hydrogen at 700 bar and 25 °C (*9*).

3. Analysis

The following assumptions are made during the design, development and analysis of the integrated hydrogen and electrical power production system consisting of a SCWR, a four-step Cu-Cl cycle, a HCS, and a PSR:

- All components operate at steady-state conditions.
- The startup period is not considered.
- The changes in gravitational and kinetic energies are neglected.
- The electrical generator energy efficiency (η_{gen}) is 95%.
- The heat losses are neglected in heat exchangers.
- The pressure drops are neglected in heat exchangers.
- The heat losses are neglected in turbines and compressors.

The reference environment conditions are taken to be 25 °C and 1 atm. A successful simulation of the integrated system requires a proper selection of property methods for the different categories of materials involved. The following property methods are used for the integrated system:

Table 2
Materials in copper-chlorine hybrid thermochemical water decomposition cycle and their properties, and correlations used in the developed copper-chlorine cycle Aspen Plus simulation model, for temperature range of 298–675 K and at 1 atm.

Material	Copper oxychloride (Cu_2OCl_2, melanothallite)						
Parameter	Value or correlation[a]						Reference
Molecule formation	$\Delta_f H^o = -384.65 \pm 2.5$ kJ/mol; $\Delta_f S^o = 154.352$ J/mol K; $\Delta_f G^o = -369.7$ kJ/mol; $\log k_f = 64.75$; $ex_{ch} = 21.08$ kJ/mol; $c_p^o = 116.77$ kJ/kmol K; $T_o = 298.15$ K and $P_o = 1$ atm						Zamfirescu et al. and Parry [43,44]
c_p, kJ/kmol K	$a + bT + cT^2 + dT^3$; a = 53.7166572; b = 0.334033497; c = −5.22127940 × 10^{-4}; d = 2.99950910 × 10^{-7}						Zamfirescu et al. [44]
s, J/mol K	$a + b\ln(T) + cT + dT^2 + eT^3$; a = 154.352; b = 53.7166572; c = 0.334033497; d = −0.2610639700 × 10^{-3}						Zamfirescu et al. [44]
ex, J/mol	$a + bT + cT^2 + dT^3 + eT^4 + f\ln(T)$; a = 0.358948789 × 10^5; b = −45.87542993; c = 0.2448529712; d = −0.2038527680 × 10^{-3}; e = 1.3589 × 10^5; f = −16015.62134						Zamfirescu et al. [44]
Material	Cupric oxide (CuO, tenorite)						
Parameter	Value or correlation[a]						Reference
Molecule formation	$\Delta_f H^o = -156 \pm 2.1$ kJ/mol; $\Delta_f S^o = 42.59 \pm 0.4$ J/mol K; $\Delta_f G^o = -128.292$ kJ/mol; $\log k_f = 22.48$; $ex_{ch} = 6.268$ kJ/mol; $c_p^o = 42.18$ kJ/kmol K; $T_o = 298.15$ K and $P_o = 1$ atm						Zamfirescu et al. and Chase [44,45]
c_p, kJ/kmol K	$a + bT + cT^2 + dT^3 + eT^{-2}$; a = 52.465081, b = −0.0145802613, c = 4.51372247 × 10^{-5}, d = −2.91900324 × 10^{-8}; e = −816,025.22 with error$^{+0.05}_{-0.1}$ kJ/kmol K						Zamfirescu et al. [44]
s, J/mol K	$a + bT + cT^2 + dT^3 + e\ln(T) + fT^{-2}$; a = −258.3259972; b = −0.0145802613; c = 2.256861235 × 10^{-5}; d = −9.730010800 × 10^{-9}; e = 52.465081; f = 4.0801261 × 10^5						Zamfirescu et al. [44]
ex, J/mol	$a + bT + cT^2 + dT^3 + eT^4 + fT^{-1} + gT^{-2} + h\ln(T)$; a = 77,913.62262; b = 56.81218591; c = −0.01401896242; d = 0.1794674429 × 10^{-4}; e = −7.297508100 × 10^{-9}; f = 8.160252200 × 10						Zamfirescu et al. [44]
Material	Cupric chloride ($CuCl_2$, tolbachite)						
Parameter	Value or correlation[a]						Reference
Melting point	Reported value at 498 °C						Perry et al. [46]
Normal boiling point	Boiling starts when temperature is 993 °C						Perry et al. [46]
Decomposition	Melting is accompanied by decomposition of Cu_2Cl_2 at 993 °C						Perry et al. [46]
Molecule formation	$\Delta_f H^o = -218.0$ kJ/mol; $\Delta_f S^o = 108.07$ J/mol K; $\Delta_f G^o = -173.826$ kJ/mol; $\log k_f = 30.453$; $ex_{ch} = 82.474$ kJ/mol; $c_p^o = 71.88$ kJ/kmol K; $T_o = 298.15$ K and $P_o = 1$ atm						Zamfirescu et al. and Linde [44,47]
c_p, kJ/kmol K	T = 298–675 K, crystal I	$a + bT + cT^2 + dT^3 + eT^4 + fT^5$, a = −16.3596145; b = 0.750699416; c = −2.56737967 × 10^{-3}; d = 4.62107127 × 10^{-6}; e = −4.34415987 × 10^{-9}; f = 1.57231698 × 10^{-12}					Zamfirescu et al. [44]
	675–871 K, crystal II	82.4					
	For the liquid Phase, Aspen Plus library has the required data						
s, J/mol K	T = 298–675 K, crystal I	$a + bT + cT^2 + dT^3 + eT^4 + fT^5 + g\ln(T)$; a = 58.38957705; b = 0.750699416; c = −1.283689835 × 10^{-3}; d = 1.54035709 × 10^{-6}; e = −1.061039968 × 10^{-9}; f = 3.14463396 × 10^{-13}; g = −16.3596145					Zamfirescu et al. [44]
	T = 675–871 K, crystal II	172.2201546 + 82.4 ln(T/675)					
	For the liquid Phase, Aspen Plus library has the required data						
ex, J/mol	$a + bT + cT^2 + d\ln(T)$						Zamfirescu et al. [44]
	T = 298–675 K	a = 1.850096 × 10^5; b = 68.091341; c = 0.69649 × 10^{-2}; d = −21,667.1954					
	T = 675–871 K	a = 1.978071674; b = 82.4; c = 1.835569 × 10^{-9}; d = −24,567.55627					
	T = 871–1,130.75 K	a = 2.278675157; b = 100; c = −6.751777 × 10^{-9}; d = −29815.02					
Material	Cuprous chloride (CuCl, nantokite)						
Parameter	Value or correlation[a]						Reference
Melting point	Reported value at 436 °C						Knacke et al. [48]
Normal boiling point	Boiling starts when the temperature is 1221.85 °C						Chase [45]
Vapor pressure	The vapor pressure at the triple point is 10.19 Pa						Perry et al. and Linde [46,47]
	T (K)	732.15	816.15	948.15	1,187.15	1,750.15	
	P (Pa)	10	100	1000	10,000	100,000	
Molecule formation	$\Delta_f H^o = -136.816$ kJ/mol; $\Delta_f S^o = 87.446$ J/mol K; $\Delta_f G^o = -199.44$ kJ/mol; $\log k_f = 21.02$; $ex_{ch} = 75.0$ kJ/mol; $c_p^o = 53.34$ kJ/kmol K; $T_o = 298.15$ K and $P_o = 1$ atm						Zamfirescu et al. and Chase [44,45]
c_p, kJ/kmol K	T = 298–683 K	$a + bT + cT^{-2}$; a = 51.087; b = 17.656 × 10^{-3}; c = 268 × 10^3					Knacke et al. [48]
s, J/mol K	T = 298–683 K	$a + b\ln(T) + cT + dT^{-2}$; a = −210.3986829; b = 51.087; c = 0.017656; d = 1.34 × 10^5					Zamfirescu et al. [44]
ex, J/mol	T = 298–683 K	$a + bT + cT^2 + dT^{-1} + eT^{-2} + f\ln(T)$; a = 191,327.176; b = 45.823; c = 0.008828; d = 268,000; e = 3.9952 × 10^7; f = −15,231.589					Zamfirescu et al. [44]

[a] If the correlation model (i.e. $aT + bT^2 \ldots$) is not available in Aspen Plus, an excel table of T vs "variable" is produced and data is entered in Aspen Plus.

- *Steamnbs* is selected because it can accommodate supercritical water (for a temperature range of 273–2000 K and a maximum pressure of over 10,000 bar).
- The properties for solid phase materials in the Cu-Cl cycle from other sources are listed in Table 2 and are entered into Aspen Plus.
- *Solid* is used for other materials.
- Peng-Robinson (*Peng-Rob*) is used for gases.

The balance equations of mass, energy, and exergy, respectively, for the steady state process in the integrated system that are used to evaluate performance are as follows [38]:

$$\sum \dot{m}_{in} - \sum \dot{m}_{out} = 0 \tag{5}$$

$$\dot{Q}_{in} - \dot{Q}_{out} + \dot{W}_{in} - \dot{W}_{out} = \sum_{out} \dot{m}(h_{@P\&T} - h_o + h_f) - \sum_{in} \dot{m}(h_{@P\&T} - h_o + h_f) \tag{6}$$

$$\dot{E}x_{\dot{Q}_{in}} - \dot{E}x_{\dot{Q}_{out}} + \dot{E}x_{\dot{W}_{in}} - \dot{E}x_{\dot{W}_{out}} = \sum_{out} \dot{m}_{out} ex_{out} - \sum_{in} \dot{m}_{in} ex_{in} + \dot{E}x_d \tag{7}$$

$$\psi_{Cu-Cl} = \frac{\dot{m}_{H_2} ex_{H_2}}{\dot{E}x_{\dot{Q}_{net,in}} + \dot{W}_e} = \frac{\dot{m}_{S17} ex_{H_2}}{(\dot{m}_{S43} ex_{S43} - \dot{m}_{S46} ex_{S46}) + \dot{W}_e} \tag{10}$$

where $\dot{Q}_{net,in}$ is the amount of heat provided to the four-step Cu-Cl cycle by the superheated gas-like supercritical fluid, calculated as the thermal energy delivered by the supercritical fluid (based on enthalpy). The exergy content of that thermal energy is calculated as the difference in exergy flow rates provided by the supercritical fluid to the hydrolysis reactor and the Cu_2OCl_2 decomposition reactor. Note that the subscripts refer to the streams or blocks names in the Aspen Plus flow sheet for the integrated system in Fig. 3.

The second main subsystem is the PSR cycle, which receives some of its heat from the supercritical fluid and the remainder through recovering heat from other streams. Its energy and exergy efficiencies can be expressed respectively as:

$$\eta_{PSR} = \frac{(\dot{W}_{B32} - \dot{W}_{B29} - \dot{W}_{B38})}{(\dot{m}_{S50} h_{S50} + \dot{m}_{S58} h_{S58} + \dot{Q}_{B27})} \tag{11}$$

$$\psi_{PSR} = \frac{(\dot{W}_{B32} - \dot{W}_{B29} - \dot{W}_{B38})}{(\dot{m}_{S50} ex_{S50} + \dot{m}_{S58} ex_{S58} + \dot{E}x_{\dot{Q}_{B27}})} \tag{12}$$

The third main subsystem is the HCS, for which energy and exergy efficiencies respectively are as follows:

$$\eta_{HCS} = \frac{(\dot{m}^{HP}_{H_2} h^{HP}_{H_2})}{\dot{W}_C - \dot{W}_{ST} + \dot{W}_p + \dot{m}^{LP}_{H_2} h^{LP}_{H_2}} = \frac{\dot{m}_9 h_9}{\dot{W}_{C1} + \dot{W}_{C2} + \dot{W}_{C3} + \dot{W}_{C4} - \dot{W}_{ST1} - \dot{W}_{ST2} - \dot{W}_{ST3} - \dot{W}_{ST4} + \dot{W}_{P1} + \dot{W}_{P2} + \dot{W}_{P3} + \dot{W}_{P4} + \dot{m}_{S17} h_{S17}} \tag{13}$$

$$\psi_{HCS} = \frac{(\dot{m}^{HP}_{H_2}(ex^{HP}_{H_2} + +ex_{ch,H_2}))}{\dot{W}_C - \dot{W}_{ST} + \dot{W}_p + \dot{m}^{LP}_{H_2}(ex^{LP}_{H_2} + ex_{ch,H_2})} = \frac{\dot{m}_9(ex_9 + ex_{ch,H_2})}{\dot{W}_{C1} + \dot{W}_{C2} + \dot{W}_{C3} + \dot{W}_{C4} - \dot{W}_{ST1} - \dot{W}_{ST2} - \dot{W}_{ST3} - \dot{W}_{ST4} + \dot{W}_{P1} + \dot{W}_{P2} + \dot{W}_{P3} + \dot{W}_{P4} + \dot{m}_{S17}(ex_{S17} + ex_{ch,H_2})} \tag{14}$$

Here, $\dot{m}$ denotes mass flow rate, $\dot{W}$ work rate, h specific enthalpy, h_f the enthalpy of formation, ex specific exergy, and $\dot{E}x_d$ exergy destruction rate. Also, for the subscripts, in represents input, out output and o reference environment conditions. Finally, $\dot{E}x_{\dot{Q}}$ is the exergy content of the heat transfer rate $\dot{Q}$, which can be expressed as follows:

$$\dot{E}x_{\dot{Q}} = \left(1 - \frac{T_o}{T_{bs}}\right)\dot{Q} \tag{8}$$

By applying the balance equations to the integrated system and its components, corresponding energy and exergy efficiencies can be defined. The energy and exergy efficiencies of the integrated system and its main subsystems are presented next. The Cu-Cl reactors, work producing and consuming devices and all heat exchangers in the integrated system, along with their exergy efficiency and exergy destruction rate equations are listed in Tables 3a, 3b and 3c.

The first subsystem considered is the four-step Cu-Cl cycle, for which energy and exergy efficiencies respectively can be expressed as follows:

$$\eta_{Cu-Cl} = \frac{\dot{m}_{H_2} LHV_{H_2}}{\dot{Q}_{net,in} + \dot{W}_e} = \frac{\dot{m}_{S17} LHV_{H_2}}{(\dot{m}_{S43} h_{S43} - \dot{m}_{S46} h_{S46}) + \dot{W}_e} \tag{9}$$

Here, superscripts HP and LP refer to high-pressure hydrogen and low-pressure hydrogen, respectively, while the subscripts C, ST, and P denote compressor, steam turbine, and pump, respectively.

For the assessment of the overall integrated system, based on the proposed design and the selected operating parameters, the energy and exergy efficiencies are as follows:

$$\eta_{ov} = \frac{\dot{m}^{HP}_{H_2}(LHV_{H_2}) + \dot{W}_{net,out}}{\dot{Q}_{SCWR}} = \frac{\dot{m}_{S17} LHV_{H_2} + \dot{W}_{PSR} - \dot{W}_{HCS} - \dot{W}_e}{(\dot{m}_{S43} h_{S43} - \dot{m}_{S48} h_{S48})} \tag{15}$$

$$\psi_{ov} = \frac{\dot{m}^{HP}_{H_2}(ex_{H_2}) + \dot{W}_{net,out}}{\dot{E}x_{\dot{Q}_{SCWR}}} = \frac{\dot{m}_{S17} ex_{S17} + \dot{W}_{PSR} - \dot{W}_{HCS} - \dot{W}_e}{(\dot{m}_{S43} ex_{S43} - \dot{m}_{S48} ex_{S48})} \tag{16}$$

For the Cu-Cl cycle reactors, the work producing and consuming devices and all heat exchangers in the integrated system, expressions for exergy efficiency and exergy destruction rate are reported in Tables 3a, 3b and 3c. The energy efficiency is not reported because they are straightforward and simplified. For instance, since it was assumed that no heat losses occur in heat exchangers, they have 100% energy efficiencies.

4. Results and discussion

The results for the nuclear-based hydrogen and power production integrated system are reported in Table 4, including the hydrogen production rate, pressure and temperature, the overall net power output, the overall energy and exergy efficiencies, and the energy and exergy efficiencies of the subsystems of the integrated system. It is seen that the system is able to produce 2.02 kg/s of compressed hydrogen at a pressure of 700 bar and at a low temperature of 25 °C, and with a net electrical power output of 553 MW. The energy and exergy efficiencies of the HCS are 90.4% and 96.6%, respectively.

The energy and exergy efficiencies of the Cu-Cl cycle, as shown in Table 4, are 40.1% and 60.2%, respectively, which are similar to the 40.1% energy efficiency and 70% exergy efficiency found by Orhan [13] for the four-step cycle. The reason for the lower exergy efficiency in this article is that here the method of delivering the required heat is considered and the energy and exergy inputs to the cycle are based on the supercritical fluid energy and exergy. The unit thermal energy associated with the Cu-Cl cycle reactors and the heat exchangers are presented in Fig. 4. The unit thermal exergy linked to each of Cu-Cl cycle reactors and heat exchangers are shown in Fig. 5. The component in the four-step Cu-Cl cycle associated with the highest unit thermal energy is the dryer (*B14*), which is a reason for the exergy efficiency being lower than that reported in the literature. The dryer is required to convert the aqueous $CuCl_2$ to solid $CuCl_2$ by evaporating the water, and is the third step in the four-step Cu-Cl cycle. The amount of water in the aqueous solution determines the amount of thermal energy required to carry out the drying process. The amount of water should be at least the minimum amount required to dissolve the $CuCl_2$ that is produced, and is found to be 20 mol of H_2O for each 2 mol of $CuCl_2$. The second highest thermal energy supply is to the Cu_2OCl_2 decomposition reactor (*B6*). However, the component in the four-step Cu-Cl cycle that is associated with the highest unit thermal exergy is the Cu_2OCl_2 decomposition reactor, since it has to be maintained at a temperature of 530 °C and is the second highest unit thermal energy consumer. The second highest thermal exergy supply is to the dryer. Although it is maintained at relatively low temperature, the dryer requires more than twice the thermal energy than the Cu_2OCl_2 decomposition reactor. As shown in Figs. 4 and 5 the electrolysis reaction requires zero thermal energy and exergy since it is operated at environment conditions and any heat generated is allowed to transfer to the surrounding environment to maintain the reactor at 25 °C. However, as reported elsewhere [13], the four-step Cu-Cl cycle requires nearly

Table 3a
Exergy efficiency and exergy destruction rate for the four-step Cu-Cl cycle reactors, water jackets and heat exchangers.

Group	Device	Exergy efficiency	Exergy destruction rate
Reactors	B1 (hydrolysis reactor)	$\psi_{B1}=\frac{\dot{m}_{S3}ex_{S3}}{\dot{m}_{S1}ex_{S1}+\dot{m}_{S2}ex_{S2}+\dot{E}x_{\dot{Q}_{S47}}}$	$\dot{E}x_{d,B1}=(\dot{m}_{S1}ex_{S1}+\dot{m}_{S2}ex_{S2}+\dot{E}x_{\dot{Q}_{S47}})-\dot{m}_{S3}ex_{S3}$
	B6 (Cu_2OCl_2 decomposition reactor)	$\psi_{B6}=\frac{\dot{m}_{S9}ex_{S9}}{\dot{m}_{S8}ex_{S8}+\dot{E}x_{\dot{Q}_{S45}}}$	$\dot{E}x_{d,B6}=\dot{m}_{S8}ex_{S8}+\dot{E}x_{\dot{Q}_{S45}}-\dot{m}_{S9}ex_{S9}$
	B11 (electrolysis reactor)	$\psi_{B11}=\frac{\dot{m}_{S16}ex_{S16}}{\dot{W}_e+\dot{m}_{S15}ex_{S15}+\dot{m}_{S7}ex_{S7}+\dot{m}_{S14}ex_{S14}}$	$\dot{E}x_{d,B11}=\dot{W}_e+\dot{m}_{S15}ex_{S15}+\dot{m}_{S7}ex_{S7}+\dot{m}_{S14}ex_{S14}-\dot{m}_{S16}ex_{S16}$
	B14 (dryer)	$\psi_{B14}=\frac{\dot{m}_{S21}ex_{S21}+\dot{m}_{S20}ex_{S20}}{\dot{E}x_{\dot{Q}_{S40}}+\dot{m}_{S19}ex_{S19}}$	$\dot{E}x_{d,B14}=\dot{E}x_{\dot{Q}_{S40}}+\dot{m}_{S19}ex_{S19}-\dot{m}_{S21}ex_{S21}-\dot{m}_{S20}ex_{S20}$
Water jackets for heating and cooling the reactors and phase change chambers	B22 (water jacket for the dryer B14)	$\psi_{B22}=\frac{\dot{E}x_{\dot{Q}_{S40}}}{\dot{m}_{S36}ex_{S36}-\dot{m}_{S41}ex_{S41}}$	$\dot{E}x_{d,B22}=(\dot{m}_{S36}ex_{36}-\dot{m}_{41}ex_{S41})-\dot{E}x_{\dot{Q}_{S40}}$
	B26 (water jacket for the hydrolysis reactor)	$\psi_{B26}=\frac{\dot{E}x_{\dot{Q}_{S47}}}{\dot{m}_{S44}ex_{S44}-\dot{m}_{S46}ex_{S46}}$	$\dot{E}x_{d,B26}=(\dot{m}_{S44}ex_{S44}-\dot{m}_{46}ex_{S46})-\dot{E}x_{\dot{Q}_{S47}}$
	B24 (water jacket for the Cu_2OCl_2 decomposition reactor)	$\psi_{B24}=\frac{\dot{E}x_{\dot{Q}_{S45}}}{\dot{m}_{S43}ex_{S43}-\dot{m}_{S44}ex_{S44}}$	$\dot{E}x_{d,B24}=(\dot{m}_{S43}ex_{S43}-\dot{m}_{44}ex_{S44})-\dot{E}x_{\dot{Q}_{S45}}$
	B18 (water jacket for the CuCl solidifier)	$\psi_{B19}=\frac{\dot{E}x_{\dot{Q}_{S29}}}{\dot{m}_{S28}ex_{S28}-\dot{m}_{S22}ex_{S22}}$	$\dot{E}x_{d,B19}=(\dot{m}_{S28}ex_{S28}-\dot{m}_{S22}ex_{S22})-\dot{E}x_{\dot{Q}_{S29}}$
Heat exchangers	B15B5	$\psi_{B15B5}=\frac{\dot{m}_{S8}ex_{S8}-\dot{m}_{S6}ex_{S6}}{\dot{m}_{S28}ex_{S28}-\dot{m}_{S32}ex_{S32}}$	$\dot{E}x_{d,B15B5}=(\dot{m}_{S28}ex_{S28}-\dot{m}_{S32}ex_{32})-(\dot{m}_{S8}ex_{S8}-\dot{m}_{S6}ex_{S6})$
	B16B2	$\psi_{B16B2}=\frac{\dot{m}_{S1}ex_{S1}-\dot{m}_{S65}ex_{S65}}{\dot{m}_{S32}ex_{S32}-\dot{m}_{S33}ex_{S33}}$	$\dot{E}x_{d,B16B2}=(\dot{m}_{S32}ex_{S32}-\dot{m}_{S33}ex_{33})-(\dot{m}_{S1}ex_{S1}-\dot{m}_{S65}ex_{S65})$
	B39B40	$\psi_{B39B40}=\frac{\dot{m}_{S65}ex_{S65}-\dot{m}_{S4}ex_{S4}}{\dot{m}_{S60}ex_{S60}-\dot{m}_{S63}ex_{S63}}$	$\dot{E}x_{d,B16B2}=(\dot{m}_{S60}ex_{S60}-\dot{m}_{S63}ex_{63})-(\dot{m}_{S65}ex_{S65}-\dot{m}_{S4}ex_{S4})$
	B20B3	$\psi_{B20B3}=\frac{\dot{m}_{S2}ex_{S2}-\dot{m}_{S5}ex_{S5}}{\dot{m}_{S33}ex_{S33}-\dot{m}_{S36}ex_{S36}}$	$\dot{E}x_{d,B20B3}=(\dot{m}_{S33}ex_{S33}-\dot{m}_{S36}ex_{36})-(\dot{m}_{S2}ex_{S2}-\dot{m}_{S5}ex_{S5})$
	B17B10	$\psi_{B17B10}=\frac{\dot{m}_{S27}ex_{S27}-\dot{m}_{S26}ex_{S26}}{\dot{m}_{S13}ex_{S13}-\dot{m}_{S14}ex_{S14}}$	$\dot{E}x_{d,B17B10}=(\dot{m}_{S13}ex_{S13}-\dot{m}_{S14}ex_{S14})-(\dot{m}_{S27}ex_{S27}-\dot{m}_{S26}ex_{S26})$

Table 3b
Exergy efficiency and exergy destruction rate for devices in the power supporting Rankine cycle.

Group	Device	Exergy efficiency	Exergy destruction rate
Power supporting Rankine cycle	B29 (pump)	$\psi_{B29}=\frac{\dot{m}_{S51}ex_{S51}}{\dot{m}_{S61}ex_{S61}+\dot{W}_{B29}}$	$\dot{E}x_{d,B29}=\dot{m}_{S61}ex_{S61}+\dot{W}_{B29}-\dot{m}_{S51}ex_{S51}$
	B32 (steam turbine)	$\psi_{B32}=\frac{\dot{m}_{S54}ex_{S54}+\dot{W}_{B32}}{\dot{m}_{S53}ex_{S53}}$	$\dot{E}x_{d,B32}=\dot{m}_{S53}ex_{S53}-\dot{m}_{S54}ex_{S54}-\dot{W}_{B32}$
	B38 (pump)	$\psi_{B38}=\frac{\dot{m}_{S62}ex_{S62}}{\dot{m}_{S55}ex_{S55}+\dot{W}_{B38}}$	$\dot{E}x_{d,B38}=\dot{m}_{S55}ex_{S55}+\dot{W}_{B38}-\dot{m}_{S62}ex_{S62}$
	B27B30 (heat exchanger)	$\psi_{B27B30}=\frac{\dot{m}_{S53}ex_{S53}-\dot{m}_{S51}ex_{S51}}{\dot{m}_{S46}ex_{S46}-\dot{m}_{S48}ex_{S48}}$	$\dot{E}x_{d,B27B30}=(\dot{m}_{S46}ex_{S46}-\dot{m}_{S48}ex_{S48})-(\dot{m}_{S53}ex_{S53}-\dot{m}_{S51}ex_{S51})$
	B33 (condenser)	$\psi_{B33}=\frac{\dot{m}_{S54}ex_{S54}-\dot{m}_{S55}ex_{S55}}{\dot{E}x_{\dot{Q}_{B33}}}$	$\dot{E}x_{d,B33}=\dot{E}x_{\dot{Q}_{B33}}-(\dot{m}_{S54}ex_{S54}-\dot{m}_{S55}ex_{S55})$
	B35B36 (heat exchanger)	$\psi_{B35B36}=\frac{\dot{m}_{S57}ex_{S57}-\dot{m}_{S49}ex_{S49}}{\dot{m}_{S62}ex_{S62}-\dot{m}_{S58}ex_{S58}}$	$\dot{E}x_{d,B35B36}=(\dot{m}_{S62}ex_{S62}-\dot{m}_{S58}ex_{S58})-(\dot{m}_{S57}ex_{S57}-\dot{m}_{S49}ex_{S49})$
	B31 (mixer)	$\psi_{B31}=\frac{\dot{m}_{S50}ex_{S50}}{\dot{m}_{S57}ex_{S57}-\dot{m}_{S42}ex_{S42}}$	$\dot{E}x_{d,B31}=(\dot{m}_{S57}ex_{S57}-\dot{m}_{S42}ex_{S42})-\dot{m}_{S50}ex_{S50}$
	B23 (mixer)	$\psi_{B23}=\frac{\dot{m}_{S42}ex_{S42}}{\dot{m}_{S24}ex_{S24}-\dot{m}_{S41}ex_{S41}}$	$\dot{E}x_{d,B23}=(\dot{m}_{S24}ex_{S24}-\dot{m}_{S41}ex_{S41})-\dot{m}_{S42}ex_{S42}$
	B37 (separator)	$\psi_{B23}=(\dot{m}_{S61}ex_{S61})/(\dot{m}_{S50}ex_{S50})$	$\dot{E}x_{d,B37}=(\dot{m}_{S50}ex_{S50}-\dot{m}_{S61}ex_{S61})+\dot{m}_{S60}ex_{S60}$

Table 3c
Exergy efficiency and exergy destruction rate for the devices in the hydrogen compression system.

Group	Device	Exergy efficiency	Exergy destruction rate
Compressors	C1	$\psi_{C1} = \frac{\dot{m}_2 ex_2}{\dot{m}_{S17} ex_{S17} + \dot{W}_{C1}}$	$\dot{E}x_{d,C1} = \dot{m}_{S17} ex_{S17} + \dot{W}_{C1} - \dot{m}_2 ex_2$
	C2	$\psi_{C2} = \frac{\dot{m}_4 ex_4}{\dot{m}_3 ex_3 + \dot{W}_{C2}}$	$\dot{E}x_{d,C2} = \dot{m}_{S3} ex_{S3} + \dot{W}_{C2} - \dot{m}_4 ex_4$
	C3	$\psi_{C3} = \frac{\dot{m}_6 ex_6}{\dot{m}_5 ex_5 + \dot{W}_{C3}}$	$\dot{E}x_{d,C3} = \dot{m}_{S5} ex_{S5} + \dot{W}_{C3} - \dot{m}_6 ex_6$
	C4	$\psi_{C4} = \frac{\dot{m}_8 ex_8}{\dot{m}_7 ex_7 + \dot{W}_{C4}}$	$\dot{E}x_{d,C4} = \dot{m}_7 ex_7 + \dot{W}_{C4} - \dot{m}_8 ex_8$
Steam turbines	ST1	$\psi_{ST1} = \frac{\dot{W}_{ST1} + \dot{m}_{R4} ex_{R4}}{\dot{m}_{R3} ex_{R3}}$	$\dot{E}x_{d,ST1} = \dot{m}_{R3} ex_{R3} - (\dot{W}_{ST1} + \dot{m}_{R4} ex_{R4})$
	ST2	$\psi_{ST2} = \frac{\dot{W}_{ST2} + \dot{m}_{X4} ex_{X4}}{\dot{m}_{X3} ex_{X3}}$	$\dot{E}x_{d,ST2} = \dot{m}_{X3} ex_{X3} - (\dot{W}_{ST2} + \dot{m}_{X4} ex_{X4})$
	ST3	$\psi_{ST3} = \frac{\dot{W}_{ST3} + \dot{m}_{Y4} ex_{Y4}}{\dot{m}_{Y3} ex_{Y3}}$	$\dot{E}x_{d,ST3} = \dot{m}_{Y3} ex_{Y3} - (\dot{W}_{ST3} + \dot{m}_{Y4} ex_{Y4})$
	ST4	$\psi_{ST4} = \frac{\dot{W}_{ST4} + \dot{m}_{Z4} ex_{Z4}}{\dot{m}_{Z3} ex_{Z3}}$	$\dot{E}x_{d,ST4} = \dot{m}_{Z3} ex_{Z3} - (\dot{W}_{ST4} + \dot{m}_{Z4} ex_{Z4})$
Pumps	P1	$\psi_{P1} = \frac{\dot{m}_{R2} ex_{R2}}{\dot{W}_{P1} + \dot{m}_{R1-C} ex_{R1-C}}$	$\dot{E}x_{d,P1} = \dot{W}_{P1} + \dot{m}_{R1-C} ex_{R1-C} - \dot{m}_{R2} ex_{R2}$
	P2	$\psi_{P2} = \frac{\dot{m}_{X2} ex_{X2}}{\dot{W}_{P2} + \dot{m}_{X1-C} ex_{X1-C}}$	$\dot{E}x_{d,P2} = \dot{W}_{P2} + \dot{m}_{X1-C} ex_{X1-C} - \dot{m}_{X2} ex_{X2}$
	P3	$\psi_{P3} = \frac{\dot{m}_{Y2} ex_{Y2}}{\dot{W}_{P3} + \dot{m}_{Y1-C} ex_{Y1-C}}$	$\dot{E}x_{d,P3} = \dot{W}_{P3} + \dot{m}_{Y1-C} ex_{Y1-C} - \dot{m}_{Y2} ex_{Y2}$
	P4	$\psi_{P4} = \frac{\dot{m}_{Z2} ex_{Z2}}{\dot{W}_{P4} + \dot{m}_{Z1-C} ex_{Z1-C}}$	$\dot{E}x_{d,P4} = \dot{W}_{P4} + \dot{m}_{Z1-C} ex_{Z1-C} - \dot{m}_{Z2} ex_{Z2}$
Heat exchangers	HX1	$\psi_{HX1} = \frac{\dot{m}_{R3} ex_{R3} - \dot{m}_{R2} ex_{R2}}{\dot{m}_2 ex_2 - \dot{m}_3 ex_3}$	$\dot{E}x_{d,HX1} = (\dot{m}_2 ex_2 - \dot{m}_3 ex_3) - (\dot{m}_{R3} ex_{R3} - \dot{m}_{R2} ex_{R2})$
	HX2	$\psi_{HX2} = \frac{\dot{m}_{X3} ex_{X3} - \dot{m}_{X2} ex_{X2}}{\dot{m}_4 ex_4 - \dot{m}_5 ex_5}$	$\dot{E}x_{d,HX2} = (\dot{m}_4 ex_4 - \dot{m}_5 ex_5) - (\dot{m}_{X3} ex_{X3} - \dot{m}_{X2} ex_{X2})$
	HX3	$\psi_{HX3} = \frac{\dot{m}_{Y3} ex_{Y3} - \dot{m}_{Y2} ex_{Y2}}{\dot{m}_6 ex_6 - \dot{m}_7 ex_7}$	$\dot{E}x_{d,HX3} = (\dot{m}_6 ex_6 - \dot{m}_7 ex_7) - (\dot{m}_{Y3} ex_{Y3} - \dot{m}_{Y2} ex_{Y2})$
	HX4	$\psi_{HX4} = \frac{\dot{m}_{Z3} ex_{Z3} - \dot{m}_{Z2} ex_{Z2}}{\dot{m}_8 ex_8 - \dot{m}_9 ex_9}$	$\dot{E}x_{d,HX4} = (\dot{m}_8 ex_8 - \dot{m}_9 ex_9) - (\dot{m}_{Z3} ex_{Z3} - \dot{m}_{Z2} ex_{Z2})$
Condensers	Cond1	$\psi_{Cond1} = \frac{\dot{E}x_{\dot{Q}_{cond1}} + \dot{m}_{R1} ex_{R1}}{\dot{m}_{R4} ex_{R4}}$	$\dot{E}x_{d,Cond1} = \dot{m}_{R4} ex_{R4} - (\dot{E}x_{\dot{Q}_{cond1}} + \dot{m}_{R1} ex_{R1})$
	Cond2	$\psi_{Cond2} = \frac{\dot{E}x_{\dot{Q}_{cond2}} + \dot{m}_{X1} ex_{X1}}{\dot{m}_{X4} ex_{X4}}$	$\dot{E}x_{d,Cond2} = \dot{m}_{X4} ex_{X4} - (\dot{E}x_{\dot{Q}_{cond2}} + \dot{m}_{X1} ex_{X1})$
	Cond3	$\psi_{Cond3} = \frac{\dot{E}x_{\dot{Q}_{cond3}} + \dot{m}_{Y1} ex_{Y1}}{\dot{m}_{Y4} ex_{Y4}}$	$\dot{E}x_{d,Cond3} = \dot{m}_{Y4} ex_{Y4} - (\dot{E}x_{\dot{Q}_{cond3}} + \dot{m}_{Y1} ex_{Y1})$
	Cond4	$\psi_{Cond4} = \frac{\dot{E}x_{\dot{Q}_{cond4}} + \dot{m}_{Z1} ex_{Z1}}{\dot{m}_{Z4} ex_{Z4}}$	$\dot{E}x_{d,Cond4} = \dot{m}_{Z4} ex_{Z4} - (\dot{E}x_{\dot{Q}_{cond4}} + \dot{m}_{Z1} ex_{Z1})$

Table 4
Overall hydrogen production rate, pressure and temperature, overall net power output, overall system energy and exergy efficiencies, and energy and exergy efficiencies of subsystems of the integrated system.

Parameter	Symbol	Value	Unit
Overall hydrogen production rate	$\dot{m}_{H_2}$	2.02	kg/s
Temperature of product hydrogen	T_{H_2}	25.0	°C
Pressure of product hydrogen	P_{H_2}	700	bar
Overall net power produced	$\dot{W}_{net}$	553	MW
Integrated system overall energy efficiency	η_{ov}	31.6	%
Integrated system overall exergy efficiency	ψ_{ov}	56.2	%
Integrated system overall exergy destruction rate	$\dot{E}x_{d,ov}$	630	MW
Four-step Cu-Cl cycle energy efficiency	η_{Cu-Cl}	40.1	%
Four-step Cu-Cl cycle exergy efficiency	ψ_{Cu-Cl}	60.2	%
Power supporting Rankine cycle energy efficiency	η_{PSR}	36.1	%
Power supporting Rankine cycle exergy efficiency	ψ_{PSR}	70.8	%
Hydrogen compression system energy efficiency	η_{HCS}	35.8	%
Hydrogen compression system exergy efficiency	ψ_{HCS}	96.6	%

55.0 kJ/mol H_2 of electrical power. The exergy efficiencies and the unit exergy destruction rates associated with the components of the four-step Cu-Cl cycle are presented in Fig. 6. The Cu_2OCl_2 decomposition reactor is seen there to be the component with the highest unit exergy destruction rate, at 85.2 kJ/mol H_2. This is expected since that device has the highest unit thermal exergy interaction in the Cu-Cl cycle. The second highest unit exergy destruction is attributable to the water jacket of the CuCl solidification reactor (*B18*), at 54.8 kJ/mol H_2. Since the solidification of CuCl first starts from molten CuCl at 530 °C and then the latent heat released at a relatively high temperature of 436 °C, compared to the 100 °C temperature of the thermal energy absorbing fluid (water), which means high-quality heat is used for a process requiring lower quality thermal energy. The lowest unit exergy destruction rate is associated with the exchangers B5 and B40, since the unit thermal exergy associated with each of these reactors is low compared to the cycle reactors.

The PSR has an energy efficiency of 36.1% and an exergy efficiency of 70.8%, as shown in Table 4. The PSR is able to produce the electrical power required by the Cu-Cl cycle and the HCS, and also to export 553 MW of electrical power to the grid. The main components of the PSR are shown in Figs. 1 and 3, while the component exergy efficiencies and unit exergy destruction rates are shown in Fig. 7. The component with the highest unit exergy destruction rate is the steam turbine (*B32*), at 304 kJ/mol H_2, which is expected since it has the highest energy interaction between the component of the SPR system. The component with the second highest unit exergy destruction rate is the boiler (*B27* and *B30*), in which thermal energy with high quality (minimum temperature of 350 °C) is used to raise the temperature of water from 100 °C. The lowest unit exergy destruction rate is the condenser, since the thermal energy is rejected at low constant temperature and the fluid experiences only phase change, for which the exergy efficiency is high.

The exergy efficiency and the unit exergy destruction rate of the work producing and consuming components in the HCS are shown in Fig. 8a. The three pumps have exergy efficiencies that are comparable to those of the other work producing and consuming devices in the HCS system. The highest unit exergy destruction is attributable to the first compressor in the four-stage hydrogen compression system. This is because it starts compressing the hydrogen from the dead state conditions, which means that the total exergy input to the compressor is just the work rather than having two exergy inputs, since the physical exergy of hydrogen at the dead state conditions is equal to zero. The exergy efficiencies and the unit exergy destruction of the heat exchangers and the condensers in the HCS system are shown in Fig. 8b. The unit exergy destruction of the main three subsystems are shown in Fig. 9,

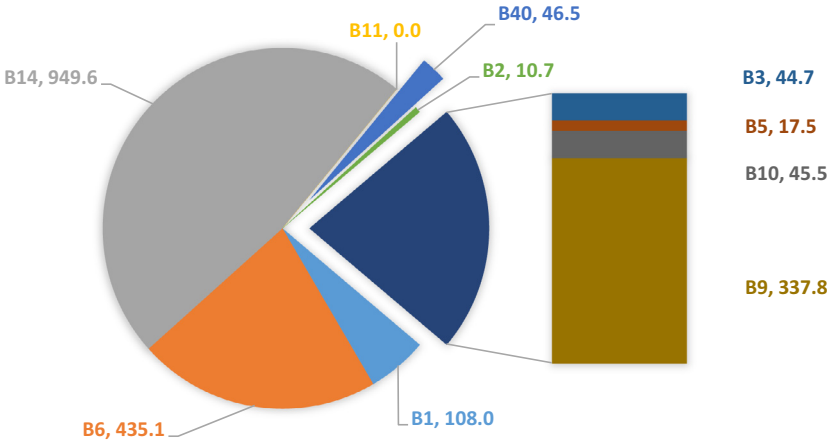

Fig. 4. Breakdown of unit thermal energy ($\dot{Q}/\dot{n}_{H_2}$) (represented by second value for each item and in kJ/mol H_2) associated with each of Cu-Cl cycle reactors and heat exchangers (identified by first alphanumeric indicator for each item). Refer to Fig. 3 for the location of each of the components in the figure.

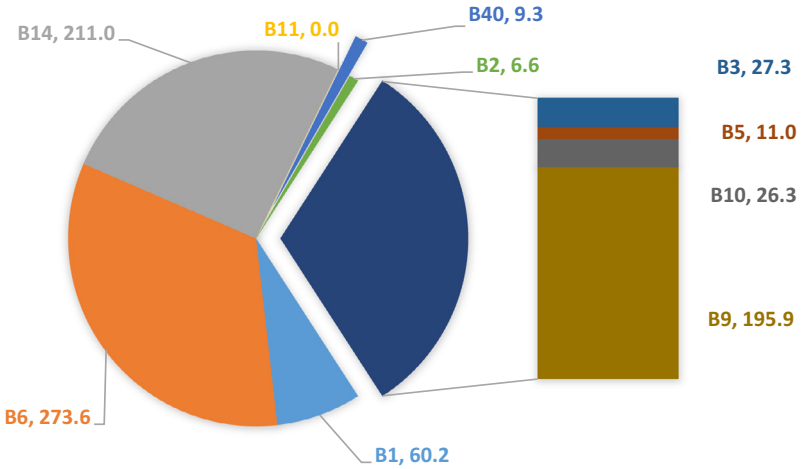

Fig. 5. Breakdown of unit thermal exergy ($\dot{E}x_{\dot{Q}}/\dot{n}_{H_2}$) (represented by second value for each item and in kJ/mol H_2) associated with each of Cu-Cl cycle reactors and heat exchangers (identified by first alphanumeric indicator for each item). Refer to Fig. 3 for the location of each of the components in the figure.

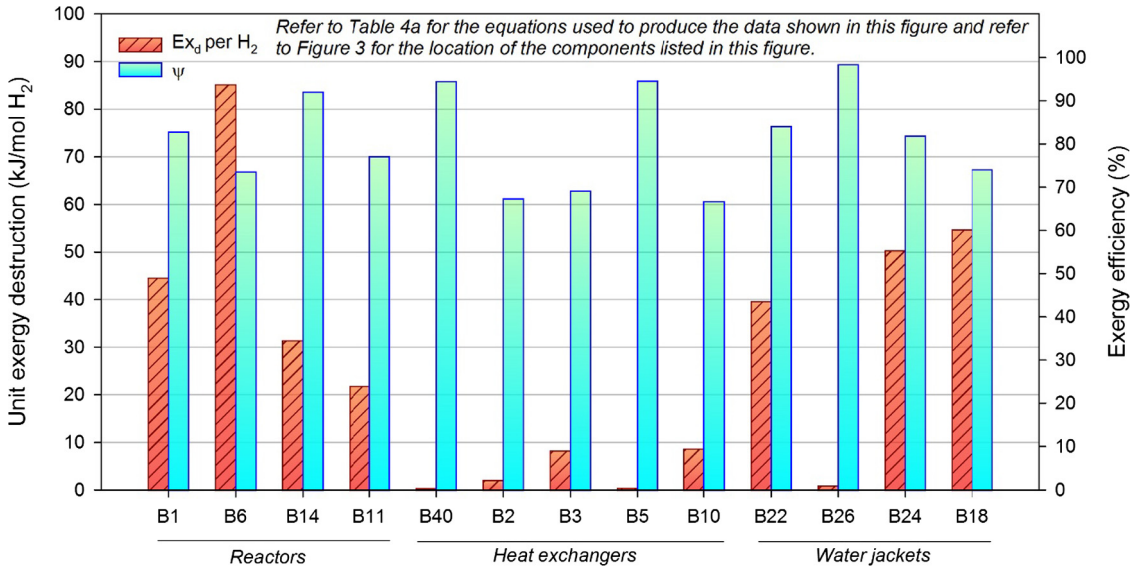

Fig. 6. Exergy efficiency and unit exergy destruction associated with each of the components of the four-step Cu-Cl cycle.

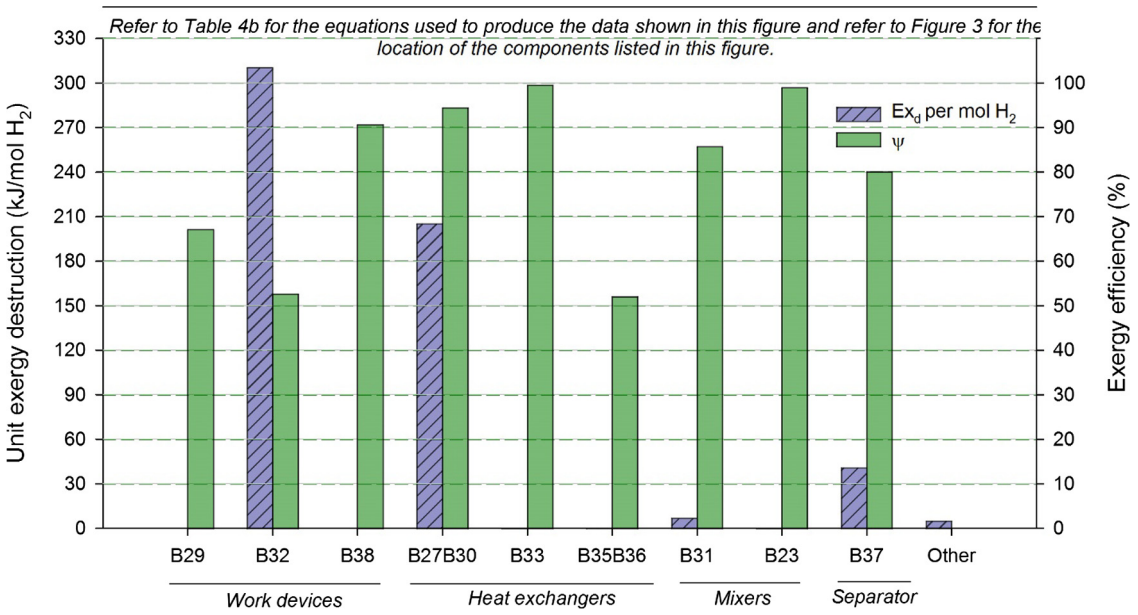

Fig. 7. Exergy efficiency and unit exergy destruction of the components of the PSR.

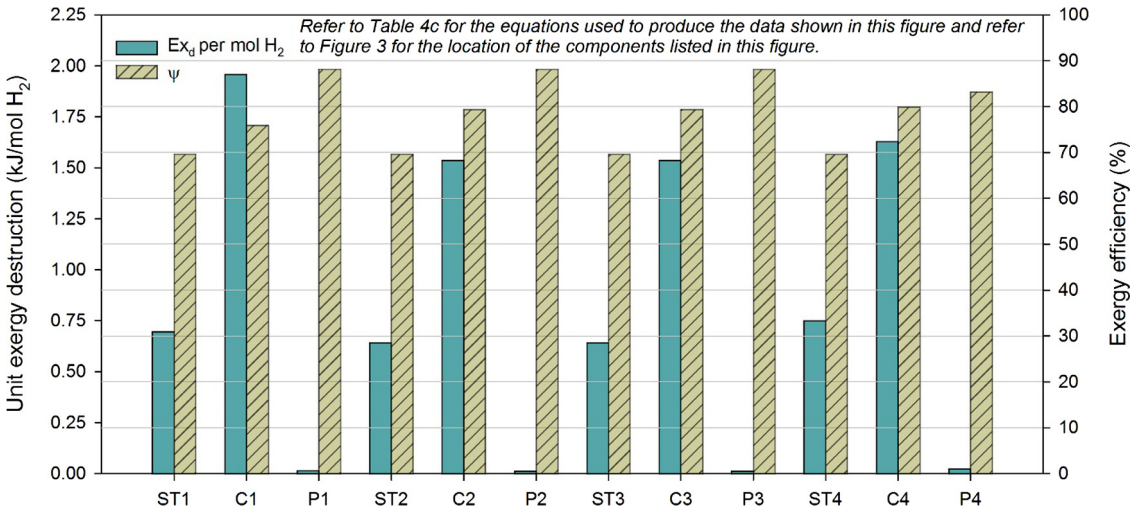

Fig. 8a. Exergy efficiency and unit exergy destruction of the work producing and consuming components in the HCS.

where the subsystem with the greatest unit exergy destruction rate in the integrated system is seen to be the PSR.

5. Conclusions

A novel nuclear-based integrated system for electrical power and compressed hydrogen production plant is proposed. The hydrogen is produced through the four-step hybrid thermochemical water decomposition cycle that utilizes copper and chlorine compounds. A Rankine cycle is used to generate power, part of which is used by the electrolysis step in the hybrid thermochemical water decomposition cycle and the hydrogen compression system. The nuclear heat is delivered to the other systems in the integrated system in the form of supercritical fluid. The nuclear reactor is based on a supercritical water-cooled reactor with a closed loop containing the supercritical fluid. The integrated system is simulated using the process engineering software Aspen Plus. The integrated system performance is assessed through energy and exergy analyses, demonstrating the following:

- The energy and exergy efficiencies of the proposed system are 31.6% and 56.2%, respectively.
- The nuclear-based integrated system is able to produce 2.02 kg/s of highly compressed hydrogen at 700 bar, and 553 MW of electrical power.
- The subsystem that destroys the most exergy in the integrated system is the power supporting Rankine cycle, at 463 kW/mol H_2.

Based on the results of the integrated system, it is concluded that the idea of integrating nuclear reactors with high temperature output to produce hydrogen has promise, and is supported by the reasonable energy and exergy efficiencies. However, further studies replacing the power supporting Rankine cycle with a more efficient system appear to be merited. A potential replacement for the

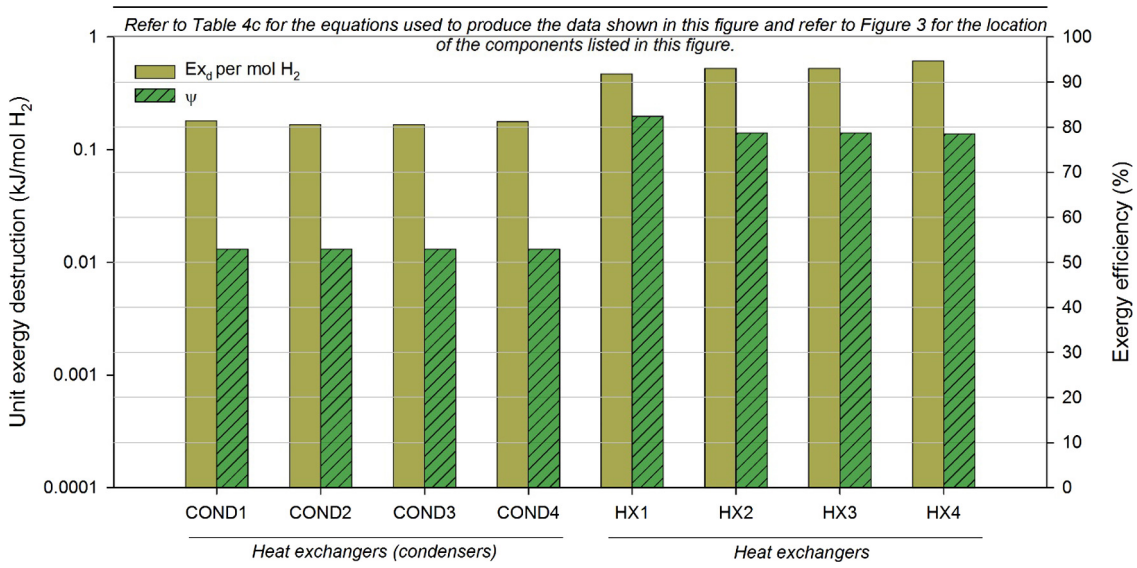

Fig. 8b. Exergy efficiency and unit exergy destruction of the condensers and heat exchangers in the HCS.

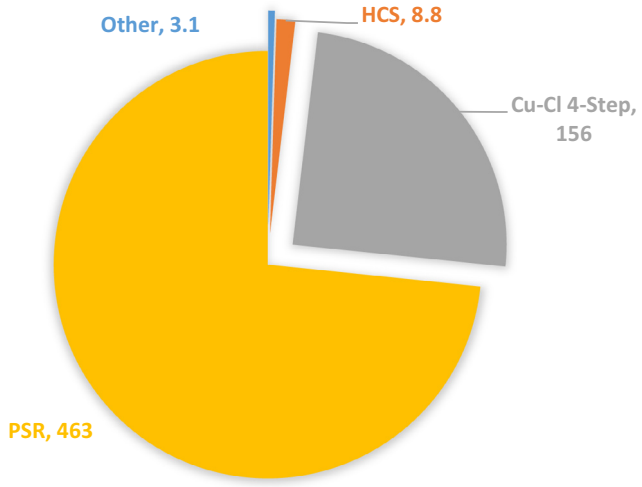

Fig. 9. Breakdown of unit thermal exergy destruction (represented by second value for each item and in kJ/mol H_2) associated with each of main subsystems in the nuclear-based integrated system.

power supporting Rankine cycle is a solid oxide fuel cell, since that would allow most of the thermal energy received from the nuclear reactor to be transferred to the hybrid thermochemical and electrical water decomposition reactor and part of the produced hydrogen would be conveyed to the solid oxide fuel cell that is also heated by the nuclear thermal energy. Carbon-free nuclear hydrogen production can mitigate carbon emissions to the environment.

Acknowledgement

The authors acknowledge the support provided by the Natural Sciences and Engineering Research Council of Canada.

References

[1] Naterer GF, Dincer I, Zamfirescu C. Hydrogen production from nuclear energy. Springer; 2013.
[2] The Monthly Energy Review. U.S. Energy Information Administration; April 2016. DOE/EIA-0035(2016/4).
[3] Dincer I, Zamfirescu C. Sustainable energy systems and applications. Springer; 2012.
[4] Dincer I, Zamfirescu C. Sustainable hydrogen production. Elsevier; 2016.
[5] Ozcan H, Dincer I. Modeling of a new four-step magnesium-chlorine cycle with dry HCl capture for more efficient hydrogen production. Int J Hydrogen Energy 2016;41:7792–801.
[6] Ozcan H, Dincer I. Performance investigation of magnesium-chloride hybrid thermochemical cycle for hydrogen production. Int J Hydrogen Energy 2014;39:76–85.
[7] Ozcan H, Dincer I. Thermodynamic modeling of a nuclear energy based integrated system for hydrogen production and liquefaction. Comput Chem Eng 2016;90:234–46.
[8] Ozcan H, Dincer I. Exergoeconomic optimization of a new four-step magnesium-chlorine cycle. Int J Hydrogen Energy 2016. http://dx.doi.org/10.1016/j.ijhydene.2016.03.098.
[9] Orhan MF, Dincer I, Rosen MA. Efficiency comparison of various design schemes for copper-chlorine (Cu-Cl) hydrogen production processes using Aspen Plus software. Energy Convers Manage 2012;63:70–86.
[10] Orhan MF, Dincer I, Rosen MA. Energy and exergy assessments of the hydrogen production step of a copper–chlorine thermochemical water splitting cycle driven by nuclear-based heat. Int J Hydrogen Energy 2008;33:6456–66.
[11] Orhan MF, Dincer I, Rosen MA. Exergoeconomic analysis of a thermochemical copper–chlorine cycle for hydrogen production using specific exergy cost (SPECO) method. Thermochim Acta 2010;497:60–6.
[12] Orhan MF, Dincer I, Rosen MA. Simulation and exergy analysis of a copper-chlorine thermochemical water decomposition cycle for hydrogen production. In: Progress in exergy, energy, and the environment. Springer; 2014. p. 121–32.
[13] Orhan MF. Conceptual design, analysis and optimization of nuclear-based hydrogen production via copper-chlorine thermochemical cycles. Faculty of Engineering and Applied Science, Mechanical Engineering Program. University of Ontario Institute of Technology, Oshawa, Canada; 2011.
[14] Orhan MF, Dincer I, Rosen MA. Efficiency analysis of a hybrid copper-chlorine (Cu-Cl) cycle for nuclear-based hydrogen production. Chem Eng J 2009;155:132–7.
[15] Orhan MF, Dincer I, Rosen MA. Design and simulation of a UOIT copper-chlorine cycle for hydrogen production. Int J Energy Res 2013;37:1160–74.
[16] Ozbilen A, Dincer I, Rosen MA. Development of a four-step Cu–Cl cycle for hydrogen production – Part I: Exergoeconomic and exergoenvironmental analyses. Int J Hydrogen Energy 2016;41:7814–25.
[17] Ozbilen A, Dincer I, Rosen MA. Development of new heat exchanger network designs for a four-step Cu-Cl cycle for hydrogen production. Energy 2014;77:338–51.
[18] Ozbilen A, Dincer I, Rosen MA. Development of a four-step Cu–Cl cycle for hydrogen production – Part II: Multi-objective optimization. Int J Hydrogen Energy 2016;41:7826–34.
[19] Ferrandon MS, Lewis M, Tatterson DF, Nankani RV, Kumar M, Wedgewood L, et al. The hybrid Cu–Cl thermochemical cycle. I. Conceptual process design and H2A cost analysis. II. Limiting the formation of CuCl during hydrolysis. In: NHA annual hydrogen conference. p. 1–20.
[20] Orhan MF, Dincer I, Rosen MA. The oxygen production step of a copper–chlorine thermochemical water decomposition cycle for hydrogen production: energy and exergy analyses. Chem Eng Sci 2009;64:860–9.
[21] Pope K, Wang Z, Naterer GF. Process integration of material flows of copper chlorides in the thermochemical Cu–Cl cycle. Chem Eng Res Des 2016;109:273–81.

[22] Ghandehariun S, Naterer GF, Rosen MA, Wang Z. Indirect contact heat recovery with solidification in thermochemical hydrogen production. Energy Convers Manage 2014;82:212–8.
[23] Wang Z, Naterer GF, Gabriel K. Multiphase reactor scale-up for Cu-Cl thermochemical hydrogen production. Int J Hydrogen Energy 2008;33:6934–46.
[24] Ratlamwala TAH, Dincer I. Experimental study of a hybrid photocatalytic hydrogen production reactor for Cu-Cl cycle. Int J Hydrogen Energy 2014;39:20744–53.
[25] Ferrandon MS, Lewis MA, Alvarez F, Shafirovich E. Hydrolysis of $CuCl_2$ in the Cu-Cl thermochemical cycle for hydrogen production: experimental studies using a spray reactor with an ultrasonic atomizer. Int J Hydrogen Energy 2010;35:1895–904.
[26] Granovskii M, Dincer I, Rosen MA, Pioro I. Performance assessment of a combined system to link a supercritical water-cooled nuclear reactor and a thermochemical water splitting cycle for hydrogen production. Energy Convers Manage 2008;49:1873–81.
[27] Ratlamwala TAH, Dincer I. Performance assessment of solar-based integrated Cu-Cl systems for hydrogen production. Solar Energy 2013;95:345–56.
[28] Dincer I, Ratlamwala TAH. Development of novel renewable energy based hydrogen production systems: a comparative study. Energy Convers Manage 2013;72:77–87.
[29] Ratlamwala TAH, Dincer I. Comparative energy and exergy analyses of two solar-based integrated hydrogen production systems. Int J Hydrogen Energy 2015;40:7568–78.
[30] Aghahosseini S, Dincer I, Naterer GF. Integrated gasification and Cu-Cl cycle for trigeneration of hydrogen, steam and electricity. Int J Hydrogen Energy 2011;36:2845–54.
[31] Wu W, Felicia W. Heat integration of a hydrogen production system with simplistic copper-chlorine (Cu-Cl) thermochemical cycle. In: 5th International symposium on advanced control of industrial processes. p. 143–6.
[32] Orhan MF, Dincer I, Rosen MA, Kanoglu M. Integrated hydrogen production options based on renewable and nuclear energy sources. Renew Sust Energy Rev 2012;16:6059–82.
[33] Ratlamwala TAH, Dincer I. Energy and exergy analyses of a Cu–Cl cycle based integrated system for hydrogen production. Chem Eng Sci 2012;84:564–73.
[34] Naterer G, Suppiah S, Lewis M, Gabriel K, Dincer I, Rosen MA, et al. Recent Canadian advances in nuclear-based hydrogen production and the thermochemical Cu-Cl cycle. Int J Hydrogen Energy 2009;34:2901–17.
[35] Naterer GF, Suppiah S, Stolberg L, Lewis M, Wang Z, Dincer I, et al. Progress of international hydrogen production network for the thermochemical Cu-Cl cycle. Int J Hydrogen Energy 2013;38:740–59.
[36] Dincer I, Naterer GF. Overview of hydrogen production research in the Clean Energy Research Laboratory (CERL) at UOIT 2014. Int J Hydrogen Energy 2014;39:20592–613.
[37] Duffey RB, Pioro IL. Supercritical water-cooled nuclear reactors: review and status. Nuclear energy materials and reactors. In: Nuclear materials and reactors from encyclopedia of life support systems (EOLSS), developed under the Auspices of the UNESCO. Oxford: EOLSS Publishers; 2005.
[38] Dincer I, Rosen MA. Exergy: energy, environment and sustainable development. 2nd ed. Elsevier; 2012.
[39] Bushby SJ, Dimmick GR, Duffey RB, Spinks NJ, Burrill KA, Chan PSW. Conceptual designs for advanced, high-temperature CANDU reactors. In: The 1st international symposium on supercritical water-cooled reactor design and technology (SCR-2000). p. 29–36.
[40] Boggs BK, Botte GG. On-board hydrogen storage and production: an application of ammonia electrolysis. J Power Sources 2009;192:573–81.
[41] Toyota Canada: Toyota to Increase "Mirai" Production; 2014. <http://www.toyota.ca/toyota/en/company-info/news/post/toyota-to-increase-mirai-production> (accessed September 13, 2016).
[42] Nguyen-Schäfer H. Rotordynamics of automotive turbochargers. Springer; 2012.
[43] Parry T. Thermodynamics and magnetism of Cu_2OCl_2. Masters dissertation, Department of Chemistry and Biochemistry. Brigham Young University, Provo, Utah; December 2008.
[44] Zamfirescu C, Dincer I, Naterer GF. Thermophysical properties of copper compounds in copper-chlorine thermochemical water splitting cycles. Int J Hydrogen Energy 2010;35:4839–52.
[45] Chase Jr MW. NIST-JANAF thermochemical tables. J Phys Chem Ref Data, Monograph 1998;9. 4th ed..
[46] Perry RH, Green DW, Maloney JO. Perry's chemical engineers' handbook. McGraw-Hill; 1984.
[47] Lide DR. CRC handbook of chemistry and physics: a ready-reference book of chemical and physical data. CRC Press; 2008.
[48] Knacke O, Kubaschewski O, Hesselmann K. Thermochemical properties of inorganic substances. Springer-Verlag; 1991.